Check for updates

Mathematical Methods in the Applied Sciences

WILEY

RESEARCH ARTICLE OPEN ACCESS

Numerical Investigation of a Diffusive SIR Model: Focus on Positivity Preservation

Rahele Mosleh[1] | Claudia Panico[2] | Messoud Efendiyev[3,4,5]

[1]Laboratory for Industrial and Applied Mathematics (LIAM), York University, Toronto, Ontario, Canada | [2]Department of Mathematics and Applications, University of Naples Federico II, Naples, Italy | [3]Azerbaijan University of Architecture and Construction, Baku, Azerbaijan | [4]Department of Mathematics, Marmara University, Istanbul, Turkey | [5]Helmholtz Zentrum München, Institut für Computational Biology, Neuherberg, Germany

Correspondence: Rahele Mosleh (rmosleh@yorku.ca)

Received: 16 November 2025 | **Revised:** 2 February 2026 | **Accepted:** 6 February 2026

ABSTRACT

In this paper, we consider a system of semilinear partial differential equations (PDEs) representing a spatially extended SIR epidemic model. A brief analytical investigation of the well-posedness and positivity of the solutions is provided in the appendix, while the main focus is on the numerical treatment of the model. We examine the performance of several time-stepping schemes, including the standard forward Euler, semi-implicit Crank–Nicolson, their Mickens-type nonstandard counterparts, and explicit exponential Runge–Kutta methods. Particular attention is given to the preservation of positivity in the numerical solutions, which is crucial for maintaining biological relevance. Two step-size functions are employed, and the results are compared in terms of theoretical accuracy and computational runtime to identify the most efficient method for simulations. Our numerical results show that positivity is preserved by the standard and exponential methods only under certain restrictions on the time-step size. In contrast, the corresponding nonstandard methods maintain positivity unconditionally, regardless of the time-step size. These findings underscore the effectiveness of nonstandard schemes in modeling epidemic dynamics governed by reaction-diffusion systems.

1 | Introduction

Mathematical models based on partial differential equations (PDEs) have become indispensable tools for investigating the spatial-temporal dynamics of infectious diseases. These models enable the integration of local disease dynamics with spatial diffusion processes, thereby capturing how diseases spread across geographical regions or within spatially structured populations [1–4]. Among the most prominent PDE-based frameworks are reaction-diffusion systems of the susceptible infectious recovered (SIR) type, which have been widely used to study various epidemics in heterogeneous environments [5, 6]. Such models account for both the temporal evolution of disease compartments and the mobility of individuals through diffusion, making them suitable for simulating realistic scenarios including urban outbreaks, wildlife epidemics,

This is an open access article under the terms of the Creative Commons Attribution License, which permits use, distribution and reproduction in any medium, provided the original work is properly cited.

© 2026 The Author(s). *Mathematical Methods in the Applied Sciences* published by John Wiley & Sons Ltd.

and plant disease dissemination. A fundamental mathematical requirement in modeling infectious diseases is the positivity preserving of solutions: that is, the model solution, typically representing population densities or proportions, must remains non-negative at all times and across all spatial domains, provided the initial data are non-negative. Violating this condition leads to biologically meaningless results and can significantly impair the interpretation of simulation outputs. While analytical results often ensure positivity of the continuous model, preserving this property at the discrete (numerical) level remains a non-trivial challenge. Standard numerical methods, including classical finite difference, finite volume, and finite element approaches, while known for their consistency and convergence, may fail to maintain positivity under coarse time steps or large spatial discretizations [7, 8]. To overcome these limitations, several strategies have been developed. These include the use of adaptive mesh refinement [9], positivity-preserving flux limiters [10], the method of entropy variables [11, 12], and implicit-explicit (IMEX) schemes with modified time integration [13]. However, many of these approaches can be computationally intensive or require problem-specific tuning. An alternative and promising direction is the use of nonstandard finite difference (NSFD) schemes, originally proposed by Mickens [14, 15], which are explicitly constructed to preserve key qualitative features of the continuous model, such as positivity, boundedness, and dynamic consistency, regardless of the discretization time-step size. NSFD methods have shown excellent performance in maintaining qualitative properties in compartmental epidemic models governed by ordinary differential equations (ODEs), such as the classical SIR, SEIR, and vector-host models [15–18]. They have also been extended to models involving delay differential equations and integral formulations [19–21]. In a broader context, related discretization techniques have been successfully applied to degenerate parabolic problems, such as those arising in biofilm modeling [22, 23]. In this work, we investigate the performance of several numerical schemes, both standard and Mickens-type nonstandard, including the forward Euler, semi-implicit Crank–Nicolson, and explicit exponential Euler, when applied to a reaction diffusion SIR model. We focus in particular on the schemes' ability to preserve the positivity of the solution across various spatial and temporal discretizations. By comparing numerical solutions under different configurations, we aim to highlight the strengths and limitations of each approach and provide insights into the practical implementation of positivity-preserving methods in spatial epidemiological modeling. We employ two different step-size functions

the explicit nonstandard Runge–Kutta methods and compare their theoretical results, numerical simulations, and runtime to identify the more efficient function to solve long-term dynamical systems. This is the novelty of this work. The remainder of the paper is organized as follows. In Section 2, we introduce the diffusive SIR model and present its continuous formulation. Section 3 describes the numerical schemes under consideration, which include both standard finite difference methods, such as the forward Euler and semi-implicit Crank–Nicolson schemes, and their Mickens-type nonstandard counterparts, as well as explicit exponential Runge–Kutta methods. This section also presents and discusses the corresponding numerical results. Section 5 offers concluding remarks and discusses potential directions for future research. Finally, the appendices discuss key mathematical properties of the model, including its analytical behavior, the positivity-preserving property of the solution, and the model's well-posedness.

2 | The Model Formulation

We consider the following diffusive SIR epidemic model [24, 25], in which the functions $S(x,t)$, $I(x,t)$, and $R(x,t)$ represent the number of susceptible, infected, and recovered individuals at spatial location x and time t, respectively:

$$\begin{aligned}
\frac{\partial S}{\partial t} &= rS\left(1-\frac{S}{k}\right) - \frac{\beta SI}{1+\alpha I} + d_S\Delta S - \mu S,\\
\frac{\partial I}{\partial t} &= \frac{\beta SI}{1+\alpha I} - \gamma\frac{I}{1+\epsilon I} + d_I\Delta I - (\mu+d+\delta)I,\\
\frac{\partial R}{\partial t} &= \delta I + \gamma\frac{I}{1+\epsilon I} + d_R\Delta R - \mu R.
\end{aligned} \tag{1}$$

We assume that $(x,t)\in\Omega\times\mathbb{R}_+$, where $\Omega\subset\mathbb{R}^n$ is a connected, bounded domain with a smooth boundary $\partial\Omega$. The operator Δ, defined by $\Delta = \frac{\partial^2}{\partial x_1^2}+\cdots+\frac{\partial^2}{\partial x_n^2}$, is the Laplacian and captures spatial diffusion. Biologically, the diffusion terms $d_S\Delta S$, $d_I\Delta I$, and $d_R\Delta R$ describe the movement of susceptible, infected, and recovered individuals within the domain. This movement is not directed, but rather mimics natural spreading behavior, where individuals tend to move from areas of higher density to areas of lower density. For example, if the density of susceptible individuals is higher at a point compared to neighboring regions, they are likely to move outward, which causes a decrease in density at that point and a smoothing of the population distribution over time. The quantities d_S, d_I, and d_R indicate the diffusion rates for susceptible, infected, and recovered individuals. The term $rS\left(1-\frac{S}{K}\right)$ describes logistic growth of the susceptible population, where $r>0$ is

10991476, 0, Downloaded from https://onlinelibrary.wiley.com/doi/10.1002/mma.70610 by Helmholtz Zentrum Muenchen Deutsches Forschungszentrum, Wiley Online Library on [21/04/2026]. See the Terms and Conditions (https://onlinelibrary.wiley.com/terms-and-conditions) on Wiley Online Library for rules of use; OA articles are governed by the applicable Creative Commons License

the intrinsic growth rate and $K > 0$ is the carrying capacity. Infection occurs at a nonlinear, saturated incidence rate given by $\frac{\beta SI}{1+\alpha I}$, where $\beta > 0$ is the transmission or contact rate, and $\alpha > 0$ is a saturation constant that accounts for behavioral changes or limited contact opportunities when the number of infected individuals is high. Natural death occurs at rate $\mu > 0$, affecting all compartments. Infected individuals additionally experience a disease-induced death at rate $d > 0$, and recover naturally at rate $\delta > 0$. The treatment process is modeled by the term $\frac{\gamma I}{1+\varepsilon I}$, where $\gamma \geq 0$ is the maximal treatment rate per individual, and $\varepsilon > 0$ is a saturation parameter representing treatment delays due to limited healthcare resources or congestion. We assume that the system (1) is subject to the following initial conditions:

$$S(x,0) = S_0(x) \geq 0, \quad I(x,0) = I_0(x) \geq 0, \quad R(x,0) = R_0(x) \geq 0, \qquad x \in \Omega, \tag{2}$$

where the initial data $S_0(x)$, $I_0(x)$ and $R_0(x)$ are non-negative functions defined on the spatial domain Ω, and we assume that $S_0(x)$, $I_0(x)$ and $R_0(x)$ are Hölder continuous functions in the closure $\overline{\Omega}$. In addition, we impose homogeneous Neumann boundary conditions:

$$\frac{\partial S}{\partial \vec{n}}(x,t) = \frac{\partial I}{\partial \vec{n}}(x,t) = \frac{\partial R}{\partial \vec{n}}(x,t) = 0, \qquad x \in \partial\Omega,\ t > 0, \tag{3}$$

where $\vec{n}$ denotes the outward-pointing unit normal vector to the boundary $\partial\Omega$. These boundary conditions express the assumption that there is no flux of individuals across the boundary of the domain, meaning the population is confined within Ω. Well-posedness, positivity-preserving property, stability, and the analysis of the total population of the model are discussed in the appendix.

3 | Numerical Methods

In this section, we apply various numerical methods to solve system (1), including the standard and Mickens-type nonstandard forward Euler methods, the semi-implicit Crank–Nicolson method, and the exponential Euler method. Our aim is to compare the efficiency of these schemes in preserving the positivity of the solution, a key qualitative property of epidemiological models.

3.1 | Standard Methods

In this section, we study the positivity of the discrete solution using the standard forward Euler method and the standard semi-implicit Crank–Nicolson method. In system (1) we consider a uniform discretization of the time interval $[0, t^*] \subset \mathbb{R}_+$ using sub intervals $N \in \mathbb{N}$, where the discrete time levels are defined by $t_n = t_0 + n\Delta t$, for $n = 0, 1, \ldots, N$, and the time-step size is given by $\Delta t = \frac{t^* - t_0}{N}$. Similarly, we discretize the spatial domain $\Omega = [a, b] \subset \mathbb{R}$, assumed to be one-dimensional, into uniform sub intervals $L \in \mathbb{N}$, yielding spatial grid points $x_i = a + i\Delta x$ for $i = 0, 1, \ldots, L$, where $\Delta x = \frac{b-a}{L}$ is the spatial step size. We denote the numerical approximations of the solution variables at grid point x_i and time level t_n by $S_i^n \approx S(x_i, t_n)$, $I_i^n \approx I(x_i, t_n)$, and $R_i^n \approx R(x_i, t_n)$, where $S_i^n, I_i^n, R_i^n \in \mathbb{R}_+$ for all i and n. These quantities represent the discrete approximations of the susceptible, infected, and recovered populations, respectively, at spatial point x_i and time t_n.

3.1.1 | Standard Forward Euler Method

The standard forward Euler method of model (1) is written as

$$\begin{aligned}
\frac{S_i^{n+1} - S_i^n}{\Delta t} &= rS_i^n\left(1 - \frac{S_i^n}{k}\right) - \beta\frac{S_i^n I_i^n}{1+\alpha I_i^n} - \mu S_i^n + d_S\frac{S_{i+1}^n - 2S_i^n + S_{i-1}^n}{\Delta L^2},\\
\frac{I_i^{n+1} - I_i^n}{\Delta t} &= \beta\frac{S_i^n I_i^n}{1+\alpha I_i^n} - (\mu + d + \delta)I_i^n - \frac{\gamma I_i^n}{1+\varepsilon I_i^n} + d_I\frac{I_{i+1}^n - 2I_i^n + I_{i-1}^n}{\Delta L^2},\\
\frac{R_i^{n+1} - R_i^n}{\Delta t} &= \delta I_i^n + \frac{\gamma I_i^n}{1+\varepsilon I_i^n} - \mu R_i^n + d_R\frac{R_{i+1}^n - 2R_i^n + R_{i-1}^n}{\Delta L^2}.
\end{aligned} \tag{4}$$

For the first equation of (4) we attain

$$\begin{aligned}
S_i^{n+1} = S_i^n &+ r\Delta t S_i^n\left(1 - \frac{S_i^n}{k}\right) - \beta\Delta t\frac{S_i^n I_i^n}{1+\alpha I_i^n} + d_S\Delta t\frac{S_{i+1}^n - 2S_i^n + S_{i-1}^n}{\Delta L^2}\\
&- \mu\Delta t S_i^n,
\end{aligned}$$

10991476, 0, Downloaded from https://onlinelibrary.wiley.com/doi/10.1002/mma.70610 by Helmholtz Zentrum Muenchen Deutsches Forschungszentrum, Wiley Online Library on [21/04/2026]. See the Terms and Conditions (https://onlinelibrary.wiley.com/terms-and-conditions) on Wiley Online Library for rules of use; OA articles are governed by the applicable Creative Commons License

$$= S_i^n\left(1 + r\Delta t\left(1 - \frac{S_i^n}{k}\right) - \beta\Delta t\frac{I_i^n}{1+\alpha I_i^n} - \frac{2\Delta t}{\Delta L^2}d_S - \mu\Delta t\right)$$
$$+ d_S\frac{\Delta t}{\Delta L^2}(S_{i+1}^n + S_{i-1}^n). \tag{5}$$

We aim to consider the positivity preserving property of the solution of discrete system (4). This means if the initial solution of system (4) is non-negative, the solution remains non-negative over time interval $[0, t^*]$. For this goal, if the solution at the nth time-step size is non-negative, $S_{i-1}^n, S_i^n, S_{i+1}^n \geq 0$, then $S_i^{n+1} \geq 0$ provided that the right side of equation (5) is non-negative. The right side of equation (5) is non-negative provided that

$$S_i^n \geq -d_S\frac{\Delta t}{\Delta L^2}(S_{i+1}^n + S_{i-1}^n) - r\Delta t S_i^n\left(1 - \frac{S_i^n}{k}\right) + \beta\Delta t\frac{S_i^n I_i^n}{1+\alpha I_i^n} + \frac{2\Delta t}{\Delta L^2}d_S S_i^n + \mu S_i^n\Delta t.$$

If

$$-d_S\frac{\Delta t}{\Delta L^2}(S_{i+1}^n + S_{i-1}^n) - r\Delta t S_i^n\left(1 - \frac{S_i^n}{k}\right) + \beta\Delta t\frac{S_i^n I_i^n}{1+\alpha I_i^n} + \frac{2\Delta t}{\Delta L^2}d_S S_i^n + \mu S_i^n\Delta t \leq 0,$$

then S_i^{n+1} is non-negative unconditionally for all Δt and ΔL. Otherwise, we have

$$\Delta t \leq \frac{S_i^n}{-\frac{d_S}{\Delta L^2}(S_{i+1}^n + S_{i-1}^n) - rS_i^n\left(1 - \frac{S_i^n}{k}\right) + \beta\frac{S_i^n I_i^n}{1+\alpha I_i^n} + \frac{2d_S}{\Delta L^2}S_i^n + \mu S_i^n}.$$

This yields the following stability constraint on the time-step size

$$\Delta t \leq \frac{1}{\beta + \frac{2d_S}{\Delta L^2} + \mu}. \tag{6}$$

By applying a similar approach to the second and third equations, we obtain the results summarized in the following theorem.

Theorem 1. *The standard forward Euler method preserves the positivity of solutions to system (1) for any spatial step size, provided that the time-step size Δt satisfies $\Delta t \leq H_1$, where*

$$H_1 = \min\left(\frac{1}{\beta + \frac{2d_S}{\Delta L^2} + \mu}, \frac{1}{\mu + d + \delta + \gamma + \frac{2d_I}{\Delta L^2}}, \frac{1}{\mu + \frac{2d_R}{\Delta L^2}}\right). \tag{7}$$

3.1.2 | Standard Semi-Implicit Crank–Nicolson Method

In this section, we investigate the positivity preserving property of the solution to the discrete scheme of system (1) using the semi-implicit Crank–Nicolson method (i.e., nonlocal discretization of the implicit Crank–Nicolson method), as applied to system (1), as follows.

$$\frac{S_i^{n+1} - S_i^n}{\Delta t} = \frac{1}{2}\left[rS_i^n\left(1 - \frac{S_i^n}{k}\right) - \beta\frac{S_i^{n+1}I_i^n}{1+\alpha I_i^n} + d_S\frac{S_{i+1}^n - 2S_i^{n+1} + S_{i-1}^n}{\Delta L^2} - \mu S_i^{n+1},\right.$$
$$\left. + rS_i^n\left(1 - \frac{S_i^n}{k}\right) - \beta\frac{S_i^n I_i^n}{1+\alpha I_i^n} + d_S\frac{S_{i+1}^n - 2S_i^n + S_{i-1}^n}{\Delta L^2} - \mu S_i^n\right]$$
$$\frac{I_i^{n+1} - I_i^n}{\Delta t} = \frac{1}{2}\left[\beta\frac{S_i^{n+1}I_i^n}{1+\alpha I_i^n} - (\mu + d + \delta)I_i^{n+1} - \frac{\gamma I_i^{n+1}}{1+\epsilon I_i^n} + d_I\frac{I_{i+1}^n - 2I_i^{n+1} + I_{i-1}^n}{\Delta L^2}\right],$$
$$+ \beta\frac{S_i^n I_i^n}{1+\alpha I_i^n} - (\mu + d + \delta)I_i^n - \frac{\gamma I_i^n}{1+\epsilon I_i^n} + d_I\frac{I_{i+1}^n - 2I_i^n + I_{i-1}^n}{\Delta L^2}\Big]$$

10991476, 0, Downloaded from https://onlinelibrary.wiley.com/doi/10.1002/mma.70610 by Helmholtz Zentrum Muenchen Deutsches Forschungszentrum, Wiley Online Library on [21/04/2026]. See the Terms and Conditions (https://onlinelibrary.wiley.com/terms-and-conditions) on Wiley Online Library for rules of use; OA articles are governed by the applicable Creative Commons License

$$\frac{R_i^{n+1}-R_i^n}{\Delta t}=\frac{1}{2}\left[\delta I_i^{n+1}+\frac{\gamma I_i^{n+1}}{1+\epsilon I_i^n}-\mu R_i^{n+1}+d_R\frac{R_{i+1}^n-2R_i^{n+1}+R_{i-1}^n}{\Delta L^2}\right.$$
$$\left.+\delta I_i^n+\frac{\gamma I_i^n}{1+\epsilon I_i^n}-\mu R_i^n+d_R\frac{R_{i+1}^n-2R_i^n+R_{i-1}^n}{\Delta L^2}\right]. \tag{8}$$

By applying the standard semi-implicit Crank–Nicolson method to system (1), the positivity-preserving property is satisfied for any spatial step size ΔL and for time-step size $\Delta t \le H_2$, where This specific form of the Crank–Nicolson scheme, which we refer to as the semi-implicit Crank–Nicolson method, simplifies the investigation of the positivity-preserving property of the numerical solution to system (1). The first equation of system (8) is equivalent to

$$S_i^{n+1}=S_i^n+\frac{\Delta t}{2}\left[rS_i^n\left(1-\frac{S_i^n}{k}\right)-\beta\frac{S_i^{n+1}I_i^n}{1+\alpha I_i^n}+ds\frac{S_{i+1}^n-2S_i^{n+1}+S_{i-1}^n}{\Delta L^2}-\mu S_i^{n+1}\right]$$
$$+\frac{\Delta t}{2}\left[rS_i^n\left(1-\frac{S_i^n}{k}\right)-\beta\frac{S_i^nI_i^n}{1+\alpha I_i^n}+ds\frac{S_{i+1}^n-2S_i^n+S_{i-1}^n}{\Delta L^2}-\mu S_i^n\right].$$

Then, rearranging terms yields

$$S_i^{n+1}=\frac{S_i^n+\Delta t\ r\ S_i^n\left(1-\frac{S_i^n}{k}\right)+d_S\frac{\Delta t}{\Delta L^2}(S_{i+1}^n+S_{i-1}^n)}{1+\beta\frac{\Delta t\ I_i^n}{2(1+\alpha I_i^n)}+\frac{\Delta t}{\Delta L^2}d_S+\frac{\Delta t}{2}\mu}$$
$$+\frac{-\frac{\Delta t}{2}\beta\frac{S_i^nI_i^n}{1+\alpha I_i^n}+\frac{d_S\Delta t}{2\Delta L^2}(S_{i+1}^n-2S_i^n+S_{i-1}^n)-\frac{\Delta t}{2}\mu S_i^n}{1+\beta\frac{\Delta t\ I_i^n}{2(1+\alpha I_i^n)}+\frac{\Delta t}{\Delta L^2}d_S+\frac{\Delta t}{2}\mu} \tag{9}$$

Assuming that the solution is non-negative at spatial positions $i-1$, i, and $i+1$ and time-step n, that is, $S_{i-1}^n, S_i^n, S_{i+1}^n \ge 0$, the solution at the next time-step, S_i^{n+1}, will remain non-negative if the following expression satisfies:

$$S_i^n+\Delta t\ r\ S_i^n\left(1-\frac{S_i^n}{k}\right)+d_S\frac{\Delta t}{\Delta L^2}(S_{i+1}^n+S_{i-1}^n)-\frac{\Delta t}{2}\beta\frac{S_i^nI_i^n}{1+\alpha I_i^n}$$
$$+\frac{d_S\Delta t}{2\Delta L^2}(S_{i+1}^n-2S_i^n+S_{i-1}^n)-\frac{\Delta t}{2}\mu S_i^n\ge 0. \tag{10}$$

Therefore, if the above condition holds, it ensures that $S_i^{n+1}\ge 0$. Rearranging terms, this leads to the condition

$$S_i^n\ge\Delta t\left(-rS_i^n\left(1-\frac{S_i^n}{k}\right)-\frac{d_S}{2\Delta L^2}(S_{i+1}^n+S_{i-1}^n)\right.$$
$$\left.+\frac{\beta}{2}\frac{S_i^nI_i^n}{1+\alpha I_i^n}-\frac{d_S}{2\Delta L^2}(S_{i+1}^n-2S_i^n+S_{i-1}^n)+\frac{\mu}{2}S_i^n\right). \tag{11}$$

If

$$-rS_i^n\left(1-\frac{S_i^n}{k}\right)-\frac{d_S}{2\Delta L^2}(S_{i+1}^n+S_{i-1}^n)+\frac{\beta}{2}\frac{S_i^nI_i^n}{1+\alpha I_i^n}$$
$$-\frac{d_S}{2\Delta L^2}(S_{i+1}^n-2S_i^n+S_{i-1}^n)+\frac{\mu}{2}S_i^n\le 0,$$

then $S_i^{n+1}\ge 0$ unconditionally for any step size Δt. Otherwise, the following bound on the time-step size is required to ensure non-negativity:

$$\Delta t\le\frac{2}{\beta+\frac{2d_S}{\Delta L^2}+\mu}. \tag{12}$$

We apply the similar approach to the second and third equation and summarize the results in the following theorem.

10991476, 0, Downloaded from https://onlinelibrary.wiley.com/doi/10.1002/mma.70610 by Helmholtz Zentrum Muenchen Deutsches Forschungszentrum, Wiley Online Library on [21/04/2026]. See the Terms and Conditions (https://onlinelibrary.wiley.com/terms-and-conditions) on Wiley Online Library for rules of use; OA articles are governed by the applicable Creative Commons License

Theorem 2. *By applying the standard semi-implicit Crank–Nicolson method to system (1), the positivity-preserving property is satisfied for any spatial step size ΔL and for time-step size $\Delta t \leq H_2$, where*

$$H_2 = \min\left(\frac{2}{\beta + \frac{2d_S}{\Delta L^2} + \mu}, \frac{2}{\mu + d + \delta + \gamma + \frac{2d_I}{\Delta L^2}}, \frac{2}{\mu + \frac{2d_R}{\Delta L^2}}\right). \tag{13}$$

Remark 3.1. The semi-implicit Crank–Nicolson method exhibits first-order consistency. The semi-implicit Crank–Nicolson method is a nonlocal scheme of the standard the implicit Crank–Nicolson method in which we substitute the prior numerical values rather than the new numerical values for some variables. This modification results in a linear system for which the solution of the system is obtained explicitly without using any sub-methods [14, 26]. By a usual computation one can easily derive that the local error of the semi-implicit Crank–Nicolson scheme is $O(\Delta t)$, implying the first order consistency of the method.

3.2 | Explicit Exponential Runge–Kutta Methods

Explicit exponential Runge–Kutta (EERK) methods are effective numerical integrators for solving semilinear parabolic partial differential equations, particularly those exhibiting stiffness. These methods treat the linear part of the system exactly, through the matrix exponential, while handling the nonlinear part explicitly, making them especially suitable for problems where the linear operator dominates the stiffness. We utilize this method in solving system (1). For this aim the system is written as

$$\dot{U}(t) = AU(t) + N(U(t)), \tag{14}$$

where A is the matrix coefficient of linear terms

$$A = \begin{bmatrix} -\mu & 0 & 0 \\ 0 & -(\mu + d + \delta) & 0 \\ 0 & \delta & -\mu \end{bmatrix}$$

and $N(U(t))$ denotes the matrix of nonlinear terms and linear Laplacian operators, and $U(t)$ shows the vector solution

$$U(t) = (S(t), I(t), R(t))^T,$$

in system (1). By employing the explicit exponential Euler method

$$u_i^{n+1} = e^{\Delta t A} u_i^n + \Delta t \frac{e^{\Delta t A} - 1}{\Delta t A} N(u_i^n), \tag{15}$$

to system (1) and noting that the Euler method is a first-order method, we expand the exponential matrix $e^{\Delta t A}$ to first order. This yields

$$\begin{aligned} u_i^{n+1} = &\begin{bmatrix} 1 - \Delta t\mu & 0 & 0 \\ 0 & 1 - (\mu + d + \delta)\Delta t & 0 \\ 0 & \delta \Delta t & 1 - \Delta t\mu \end{bmatrix} u_i^n \\ &+ \begin{bmatrix} \Delta t & 0 & 0 \\ 0 & \Delta t & 0 \\ 0 & 0 & \Delta t \end{bmatrix} N(u_i^n). \end{aligned} \tag{16}$$

System (16) is written as

$$\begin{bmatrix} S_i^{n+1} \\ I_i^{n+1} \\ R_i^{n+1} \end{bmatrix} = \begin{bmatrix} 1 - \Delta t\mu & 0 & 0 \\ 0 & 1 - (\mu + d + \delta)\Delta t & 0 \\ 0 & \delta \Delta t & 1 - \Delta t\mu \end{bmatrix} \begin{bmatrix} S_i^n \\ I_i^n \\ R_i^n \end{bmatrix}$$

10991476, 0, Downloaded from https://onlinelibrary.wiley.com/doi/10.1002/mma.70610 by Helmholtz Zentrum Muenchen Deutsches Forschungszentrum, Wiley Online Library on [21/04/2026]. See the Terms and Conditions (https://onlinelibrary.wiley.com/terms-and-conditions) on Wiley Online Library for rules of use; OA articles are governed by the applicable Creative Commons License

$$+\begin{bmatrix}\Delta t & 0 & 0\\ 0 & \Delta t & 0\\ 0 & 0 & \Delta t\end{bmatrix}\begin{bmatrix} rS_i^n\left(1-\frac{S_i^n}{k}\right)-\beta\frac{S_i^nI_i^n}{1+\alpha I_i^n}+d_S\frac{S_{i+1}^n-2S_i^n+S_{i-1}^n}{\Delta L^2}\\ -\gamma\frac{I_i^n}{1+\epsilon I_i^n}+\beta\frac{S_i^nI_i^n}{1+\alpha I_i^n}+d_I\frac{I_{i+1}^n-2I_i^n+I_{i-1}^n}{\Delta L^2}\\ \gamma\frac{I_i^n}{1+\epsilon I_i^n}+d_R\frac{R_{i+1}^n-2R_i^n+R_{i-1}^n}{\Delta L^2}. \end{bmatrix} \tag{17}$$

We aim to consider the positivity of the solution of discrete system (17). We begin by considering the first equation of (17):

$$S_i^{n+1}=(1-\Delta t\mu)S_i^n+\Delta t\left(rS_i^n\left(1-\frac{S_i^n}{k}\right)-\beta\frac{S_i^nI_i^n}{1+\alpha I_i^n}+d_S\frac{S_{i+1}^n-2S_i^n+S_{i-1}^n}{\Delta L^2}\right). \tag{18}$$

We then proceed following the same steps as in the proof of Theorem 1, and obtain the following result.

Lemma 1. *Using the explicit exponential Euler method to system (1) the positivity preserving property for the solution is preserved for any spatial step-size ΔL and the time-step size $\Delta t \le H_1$ (see (7)).*

3.3 | Nonstandard Methods

In this section, we employ Mickens' nonstandard finite difference (NSFD) method [14, 15]. To this end, we define the right-hand sides of systems (4) and (8) as

$$F_S(x_{i-1},x_i,x_{i+1},t_n),\quad F_I(x_{i-1},x_i,x_{i+1},t_n),\quad \text{and}\quad F_R(x_{i-1},x_i,x_{i+1},t_n), \tag{19}$$

corresponding to the first, second, and third equations, respectively. Using this notation, the systems (4) and (8) can be rewritten as follows:

$$\begin{aligned}\frac{S_i^{n+1}-S_i^n}{\Phi_c(\Delta t)}&=F_S(x_{i-1},x_i,x_{i+1},t_n),\\ \frac{I_i^{n+1}-I_i^n}{\Phi_c(\Delta t)}&=F_I(x_{i-1},x_i,x_{i+1},t_n),\\ \frac{R_i^{n+1}-R_i^n}{\Phi_c(\Delta t)}&=F_R(x_{i-1},x_i,x_{i+1},t_n).\end{aligned} \tag{20}$$

Here, Φ_c is a positive function of Δt that serves as a modified step-size function. As shown by Faragó and Mosleh in [27], the positivity of the numerical solution is preserved for all time-step sizes when using various step-size functions. In this context, our objective is to find a suitable constant $c > 0$ such that the positivity-preserving property holds for any time-step size Δt. If we consider the specific step-size function

$$\Phi_c(\Delta t)=\begin{cases}\frac{\Delta t}{1+c\Delta t}, & \text{for}\quad c\ge 0,\\ 0, & \text{for}\quad c<0.\end{cases} \tag{21}$$

Then $\Phi_c(\Delta t)$ is monotonically decreasing with respect to c and it satisfies the following limits:

$$\lim_{c\to 0^+}\Phi_c(\Delta t)=\Delta t,\quad \lim_{c\to+\infty}\Phi_c(\Delta t)=0,\quad \text{that is,}\quad \sup\Phi_c(\Delta t)=\Delta t. \tag{22}$$

The analysis of the step-size function (21) is as follows.

$\Delta t < H$: Since $0<\Phi_c(\Delta t)\le\Delta t$, it follows that $\Phi_c(\Delta t)\le H$.

$\Delta t \ge H$: Let

$$S=\{c>0|\Phi_c(\Delta t)\le H\}. \tag{23}$$

- There exists $\varepsilon > 0$ such that for all $0 < c < \varepsilon$,

$$\Phi_c(\Delta t)\ge\Delta t\ge H,$$

so that no c in this interval belongs to the set S.

10991476, 0, Downloaded from https://onlinelibrary.wiley.com/doi/10.1002/mma.70610 by Helmholtz Zentrum Muenchen Deutsches Forschungszentrum, Wiley Online Library on [21/04/2026]. See the Terms and Conditions (https://onlinelibrary.wiley.com/terms-and-conditions) on Wiley Online Library for rules of use; OA articles are governed by the applicable Creative Commons License

- Since $\lim_{c\to+\infty} \Phi_c(\Delta t) = 0$, there exists $c_0 > 0$ such that for all $c \geq c_0$,

$$\Phi_c(\Delta t) < H,$$

which implies that all such c belong to the set S. By the greatest-lower-bound property of $\mathbb{R}$, the set S has an minimum

$$c_0 = \inf S. \tag{24}$$

This c_0 is exactly the threshold such that for all $c \geq c_0$, $\Phi_c(\Delta t) \leq H$.

Here, the quantity H serves as an upper bound associated with the Euler, semi-implicit Crank–Nicolson and explicit exponential Euler methods, typically denoted by H_1 (see (7)) and H_2 (see (13)). We summarize these arguments in the following theorem.

Theorem 3. *The step-size function* $\Phi_c(\Delta t) = \frac{\Delta t}{1+c\Delta t}$ *satisfies the following properties*:

- *If* $\Delta t < H$, *then* $\Phi_c(\Delta t) \in (0, H]$ *for all* $c > 0$.
- *If* $\Delta t \geq H$, *then there exists a constant* $c_0 > 0$ *such that* $\Phi_c(\Delta t) \in (0, H]$ *for all* $c \geq c_0$.

The constant c_0 is the exact solution to the following equation

$$H + Hc_0\Delta t - \Delta t = 0. \tag{25}$$

This condition implies that choosing $c_0 \geq \frac{1}{H}$ is a sufficient requirement to ensure the positivity-preserving property of the method for all time-step sizes.

Remark 3.2. The exact solution of equation (25) is given by

$$c_0 = \frac{\Delta t - H}{H\Delta t}, \quad \Delta t \geq H. \tag{26}$$

Remark 3.3. The step-size function proposed in [27],

$$\Phi(\Delta t) = \frac{1 - e^{-c\Delta t}}{c}, \quad c > 0, \tag{27}$$

possesses the same property as the step-size function (21) described in (22). Moreover, the function (27) yields the exact solution for any $\Delta t > 0$, whereas the exact solution corresponding to the step-size function (21) is only valid for $\Delta t \geq H$.

4 | Numerical Simulations

In this section, we validate the theoretical results through numerical simulations using both standard and Mickens-type nonstandard methods.

4.1 | Numerical Simulations for Standard Methods

In this section, we perform numerical simulations to investigate the sharpness of the upper bounds provided in Theorems 1 2 and Lemma 1. These theorems establish conditions under which the positivity of the solution is guaranteed for the numerical schemes considered. Our goal is to assess whether these bounds are not only sufficient but also necessary by observing the behavior of the numerical solution when the time-step size is chosen below, near, or above the specified thresholds. We apply various standard and nonstandard methods, including forward Euler, semi-implicit Crank–Nicolson, and explicit exponential Euler method and examine whether the positivity of the solution is maintained under different time-step sizes. Positivity, in this context, refers to the requirement that all solution components (e.g., susceptible, infected, and recovered populations) remain non-negative throughout the simulation, which is a critical property in epidemiological and biological models. In all simulations, we impose homogeneous Neumann boundary

10991476, 0, Downloaded from https://onlinelibrary.wiley.com/doi/10.1002/mma.70610 by Helmholtz Zentrum Muenchen Deutsches Forschungszentrum, Wiley Online Library on [21/04/2026]. See the Terms and Conditions (https://onlinelibrary.wiley.com/terms-and-conditions) on Wiley Online Library for rules of use; OA articles are governed by the applicable Creative Commons License

conditions on all state variables. This means that the spatial derivative of each variable vanishes at the boundaries of the spatial domain, that is, there is no flux of the population across the boundaries. Mathematically, this is expressed as:

$$\frac{\partial S}{\partial x} = \frac{\partial I}{\partial x} = \frac{\partial R}{\partial x} = 0 \quad \text{at} \quad x = 0 \text{ and } x = L.$$

We use the following parameter values and initial conditions throughout the computations:

$$\begin{aligned} &r = 10, \quad k = 100, \quad \beta = 2.45 \times 10^{-1}, \quad \alpha = 10^{-2}, \quad \gamma = 35, \\ &d = 2 \times 10^{-1}, \quad \mu = 3.7 \times 10^{-5}, \quad \delta = 10^{-1}, \quad \epsilon = 0.5, \\ &d_S = 2 \times 10^{-2}, \quad d_I = 5 \times 10^{-3}, \quad d_R = 5 \times 10^{-3}, \end{aligned} \tag{28}$$

and

$$\begin{aligned} S(x, 0) &= 20 - 5\cos(2\pi x), \\ I(x, 0) &= 5, \\ R(x, 0) &= 0. \end{aligned} \tag{29}$$

All parameter values and initial conditions used in the simulations are taken from [24], except for the parameters β, d, μ, and δ, whose values have been specifically selected by us to perform the numerical experiments aimed at analyzing the proposed numerical schemes. For all $x \in [0, L]$, the spatial domain was set to $L = 10$, and the final simulation time was taken as $t^* = 10$. The discretization was performed using the following spatial and temporal step sizes:

$$\Delta x = 0.1, \quad \Delta t = 0.1.$$

Figure 1 illustrates the solution of the system (1), obtained using the standard forward Euler method (4) with the time-step size $\Delta t = 0.1$, which satisfies the condition $\Delta t < H_1 = 9.99 \times 10^{-1}$. This simulation illustrates the validity of Theorem 1, which ensures that the numerical solution remains non-negative, provided the initial data are non-negative and the time-step size is below the critical threshold H_1. Specifically, Figure 1a shows the temporal-spatial evolution of the susceptible component S, while Figure 1b presents the spatial profiles of all components S, I, and R at time $t = 10$. These figures clearly confirm that the numerical solution possesses the positivity preservation property throughout the domain and over the entire time interval, despite the presence of nonlinear interaction terms and diffusion. This numerical result highlights the importance of choosing an appropriate time-step size when employing the forward Euler method. If the step size satisfies the bound specified in Theorem 1, the discretized system preserves the biological realism of the model by ensuring that population densities (e.g., susceptible, infected, recovered) remain non-negative, provided the initial data are non-negative, an essential requirement in epidemiological modeling.

Figure 2 presents the numerical solution of system (4) obtained using a time-step size of $\Delta t = 1$, which exceeds the positivity-preserving upper bound $H_1 = 9.99 \times 10^{-1}$ established in Theorem 1. This experiment is designed to test the sharpness of the theoretical bound by exploring what happens when the time-step size violates the condition required for positivity preservation property of the solution. As shown in Figure 2a, the susceptible component S becomes negative during the simulation, despite being initialized with strictly positive values. Similarly, Figure 2b displays the spatial profiles of all three components S, I, and R at time $t = 5$, revealing that parts of the solution fall below zero. This behavior clearly indicates a breakdown in the positivity of the solution. In conclusion, the results shown in Figures 1 and 2 demonstrate that the bound provided in Theorem 1 is not only sufficient but also *sharp*. When the time-step size Δt remains within the allowable limit $\Delta t < H_1$, the forward Euler method successfully preserves the non-negativity of the solution, which is essential for maintaining the biological interpretability of the model. However, once Δt exceeds this upper bound, the solution may become negative, even when the initial conditions are non-negative, violating the essential requirement for realistic simulations in epidemiological models. This highlights the importance of carefully selecting time-step sizes in numerical schemes to ensure the reliability and correctness of the computed solutions.

Figure 3 illustrates the numerical solution of system (1) obtained using the semi-implicit Crank–Nicolson method (8) with two different time-step sizes: $\Delta t = 0.1$ and $\Delta t = 2$. According to Theorem 2, the upper bound on the time-step size requires to ensure positivity preservation is $H_2 = 1.99$. In Figure 3a, where the time-step size satisfies $\Delta t < H_2$, the numerical solution remains strictly non-negative throughout the simulation. This confirms the theoretical guarantee provided by Theorem 2, which states that under this bound, the semi-implicit Crank–Nicolson scheme maintains the non-negative

10991476, 0, Downloaded from https://onlinelibrary.wiley.com/doi/10.1002/mma.70610 by Helmholtz Zentrum Muenchen Deutsches Forschungszentrum, Wiley Online Library on [21/04/2026]. See the Terms and Conditions (https://onlinelibrary.wiley.com/terms-and-conditions) on Wiley Online Library for rules of use; OA articles are governed by the applicable Creative Commons License

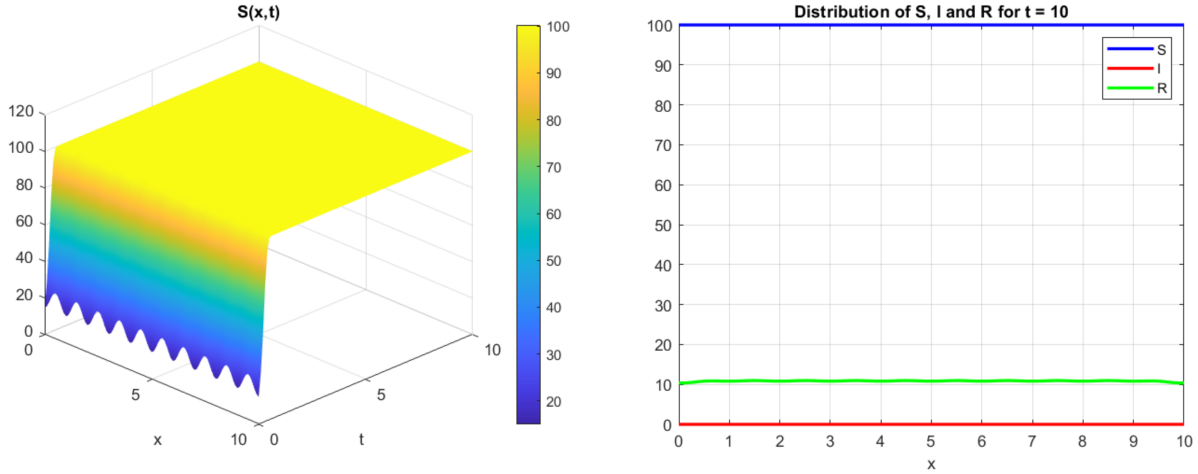

(a) (b)

FIGURE 1 | Solution of system (1) using the standard forward Euler method (4) with a time-step size below the upper bound specified in Theorem 1. (a) Time variation of the distribution of susceptible population, (b) Distribution of S, I and R for $t = 10$.

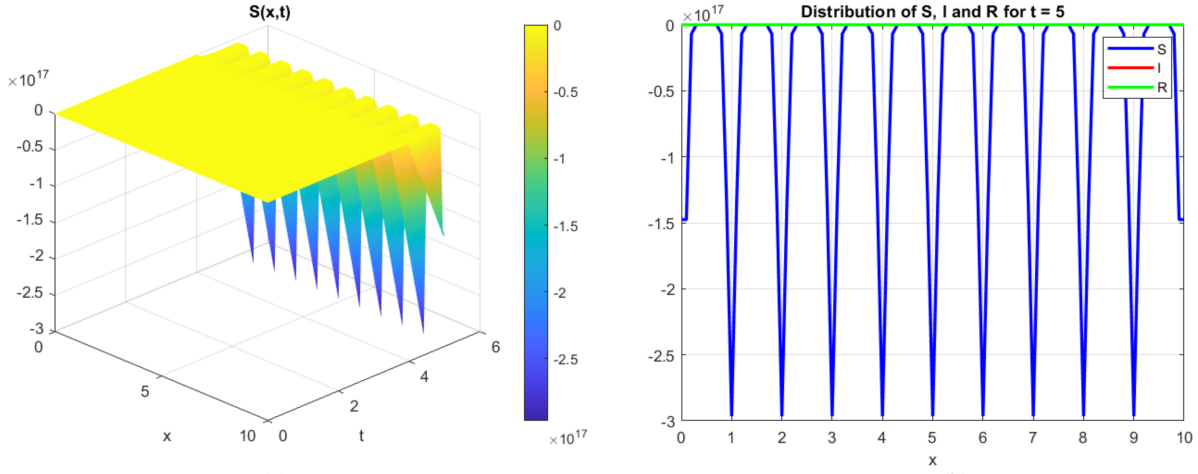

(a) (b)

FIGURE 2 | Solution of system (1) using the standard forward Euler method (4), with a time-step size that exceeds the upper bound specified in Theorem 1. (a) Time variation of the distribution of susceptible population, (b) Distribution of S, I and R for $t = 5$.

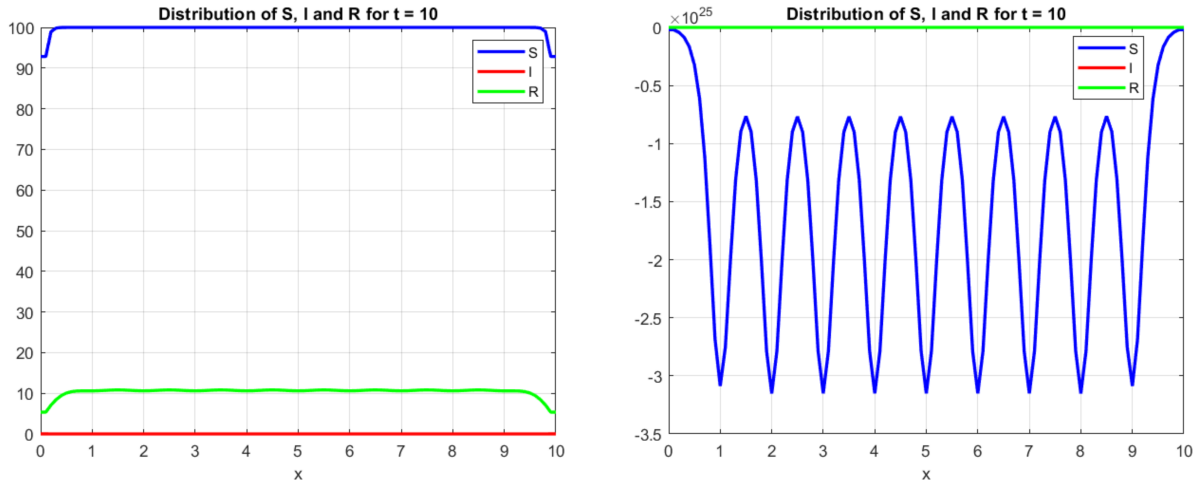

(a) (b)

FIGURE 3 | Solution of system (1) with standard semi-implicit Crank–Nicolson method (4). (a) The time-step size $\Delta t = 0.1$ satisfies the upper bound condition stated in Theorem 1. (b) The time-step size $\Delta t = 2$ exceeds the upper bound specified in Theorem 1.

10991476, 0, Downloaded from https://onlinelibrary.wiley.com/doi/10.1002/mma.70610 by Helmholtz Zentrum Muenchen Deutsches Forschungszentrum, Wiley Online Library on [21/04/2026]. See the Terms and Conditions (https://onlinelibrary.wiley.com/terms-and-conditions) on Wiley Online Library for rules of use; OA articles are governed by the applicable Creative Commons License

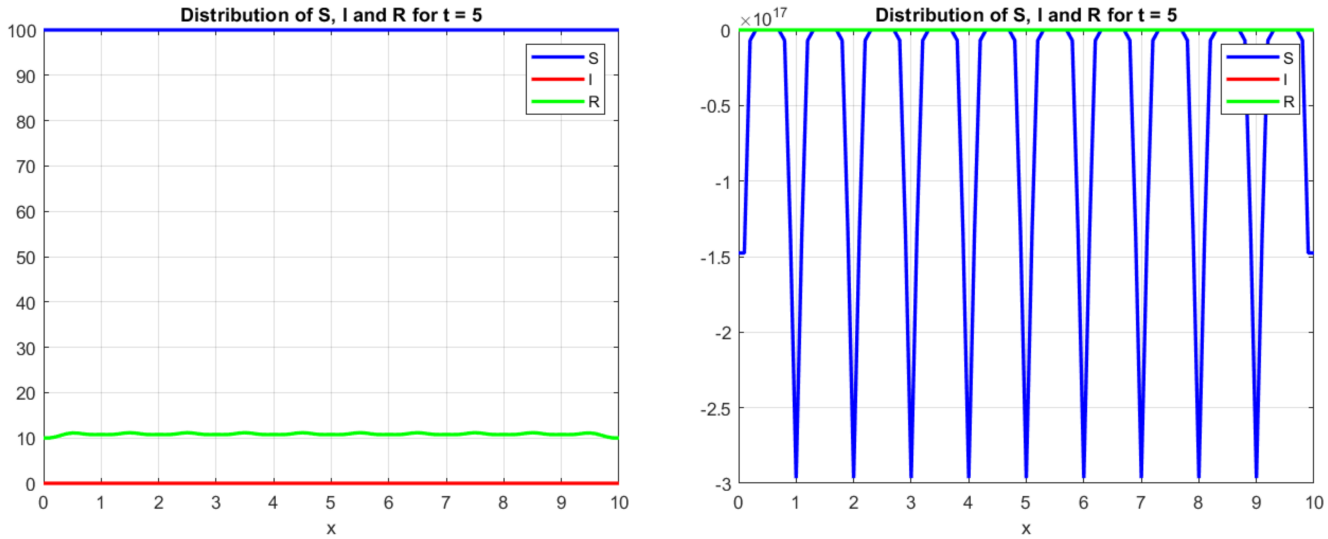

FIGURE 4 | Solution of system (1) with standard first-order explicit exponential Euler method (17). (a) The time-step size $\Delta t = 0.1$ satisfies the upper bound condition stated in Lemma 1. (b) The time-step size $\Delta t = 1$ exceeds the upper bound specified in Lemma 1.

of the solution, provided that the initial conditions are non-negative. However, as shown in Figure 3b, when the time-step size is increased to $\Delta t = 2$, which violates the bound $\Delta t < H_2$, the numerical solution loses its non-negativity. Despite the non-negative initial conditions, some components of the solution, such as the susceptible or infected populations, become negative over time. This behavior clearly indicates a breakdown in the positivity-preserving property of the scheme, underscoring the necessity of adhering to the theoretical time-step restriction. These numerical results support the sharpness and practical relevance of Theorem 2. They highlight the fact that the semi-implicit Crank–Nicolson method, while unconditionally stable in the linear case, may still fail to preserve qualitative properties such as positivity unless the time-step size is carefully chosen. This finding is particularly important in the context of epidemiological modeling, where negative population densities are biologically meaningless and can severely compromise the interpretation and precision of simulation results.

Figure 4 presents the numerical solutions of system (1), computed using the explicit exponential Euler method described in (17), for two different time-step sizes: $\Delta t = 0.1$ and $\Delta t = 1$. According to Lemma 1, the numerical scheme preserves the non-negativity of the solution if the time-step size remains below the critical threshold $H_1 = 9.99 \times 10^{-1}$. In Figure 4a, where $\Delta t = 0.1 < H_1$, the numerical solution remains strictly non-negative throughout the simulation, in agreement with the theoretical condition. This demonstrates that the explicit exponential Euler method respects the positivity-preserving property when the time-step is appropriately chosen. Conversely, in Figure 4b, with $\Delta t = 1 > H_1$, the numerical solution exhibits negative values, violating the condition outlined in Lemma 1. This highlights the importance of adhering to the theoretical step-size restriction to maintain the biological realism of the model.

4.2 | Numerical Simulations for Nonstandard Methods

In this section, we present a series of numerical experiments based on the Mickens-type nonstandard discretization scheme introduced in equation (19) for the model defined in (1). The primary objective of these simulations is twofold: first, to provide numerical evidence supporting the theoretical results on the positivity-preserving property of the solution; and second, to assess the sharpness of the derived upper bounds for the time-step size, as stated in Theorem 3. These upper bounds guarantee that the numerical solution remains non-negative when the time-step size satisfies certain conditions. To ensure consistency and reproducibility, all experiments are conducted using the fixed parameter values specified in equation (28) and the initial conditions given in equation (29).

Figure 5 illustrates the validity of Theorem 3 by presenting the solution of system (1) computed using the Mickens-type nonstandard forward Euler method (20), with the step-size function defined in (21) and a time step $\Delta t = 1$. As established in Theorem 3, choosing $c \geq c_0$, where c_0 is defined in (26), is a sufficient condition to ensure that the method preserves positivity for any time step. In this specific case, we have $c_0 = 3.65 \times 10^{-5}$ and $c = c_0 + 10$. Figures 5a and 5b show, respectively, the time evolution of the distribution of the susceptible population and the spatial distributions

10991476, 0, Downloaded from https://onlinelibrary.wiley.com/doi/10.1002/mma.70610 by Helmholtz Zentrum Muenchen Deutsches Forschungszentrum, Wiley Online Library on [21/04/2026]. See the Terms and Conditions (https://onlinelibrary.wiley.com/terms-and-conditions) on Wiley Online Library for rules of use; OA articles are governed by the applicable Creative Commons License

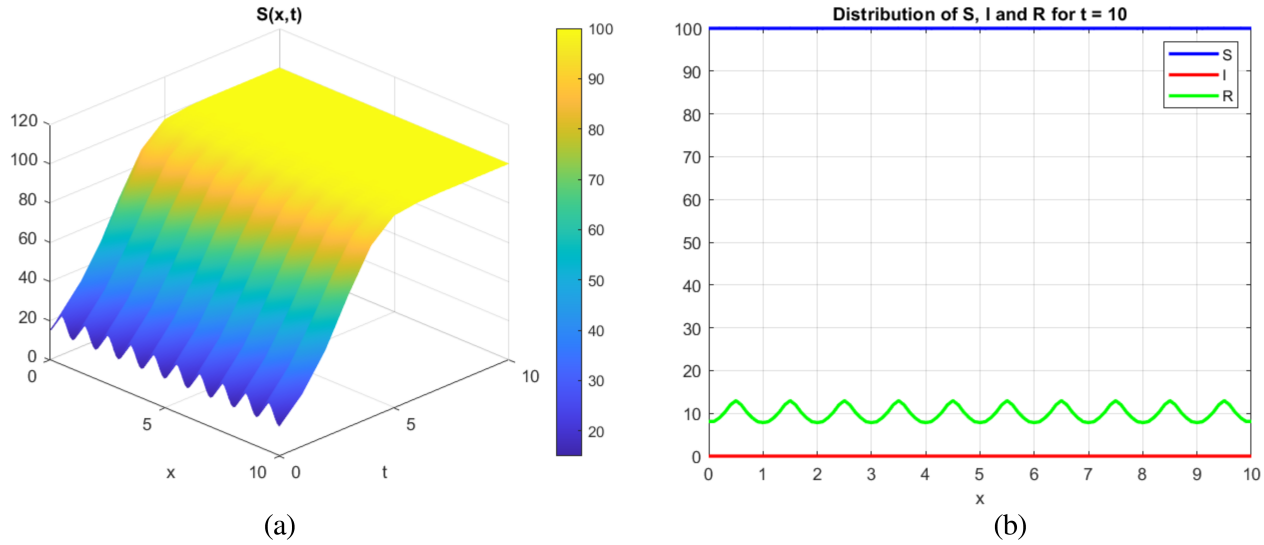

FIGURE 5 | Solution of system (1) with nonstandard Euler method (19), step-size function (21), and $\Delta t = 1$. (a) Time variation of the distribution of susceptible population, (b) Distribution of S, I and R for $t = 10$.

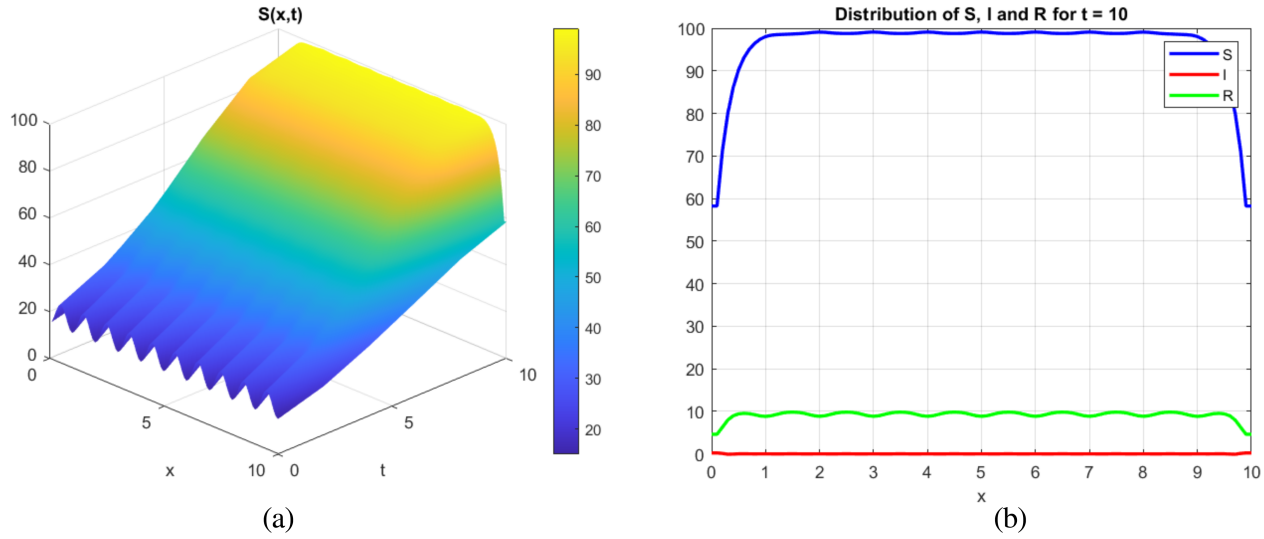

FIGURE 6 | Solution of system (1) with nonstandard semi-implicit Crank–Nicolson method (19), step-size function (21), and $\Delta t = 2$. (a) Time variation of the distribution of susceptible population, (b) Distribution of S, I and R for $t = 10$.

of S, I, and R at time $t = 10$. As can be observed from the figures, the solution remains positive throughout the simulation.

The same experiment is now performed using the nonstandard semi-implicit Crank–Nicolson method with $\Delta t = 2$. As shown in Figure 6a,b, the solution remains positive, confirming the theoretical result stated in Theorem 3. In this case, we have $c_0 = 1.83 \times 10^{-5}$ defined in equation (26), and $c = c_0 + 10$. As a final experiment, we compare the results shown in Figures 5 and 6 with those obtained using the Mickens-type nonstandard method, applying both the Euler and semi-implicit Crank–Nicolson discretizations, with the step-size function defined in (27).

Figure 7 illustrates the solution of system (1) computed using the Mickens' nonstandard forward Euler method (20), with the step-size function defined in (27) and a time step $\Delta t = 1$. In this case, we have $H_1 = 9.99 \times 10^{-1}$ and we assume $c = 1.10 \times 10^{1}$. Figures 7a and 7b show, respectively, the time evolution of the distribution of the susceptible population and the spatial distributions of S, I, and R at time $t = 10$.

10991476, 0, Downloaded from https://onlinelibrary.wiley.com/doi/10.1002/mma.70610 by Helmholtz Zentrum Muenchen Deutsches Forschungszentrum, Wiley Online Library on [21/04/2026]. See the Terms and Conditions (https://onlinelibrary.wiley.com/terms-and-conditions) on Wiley Online Library for rules of use; OA articles are governed by the applicable Creative Commons License

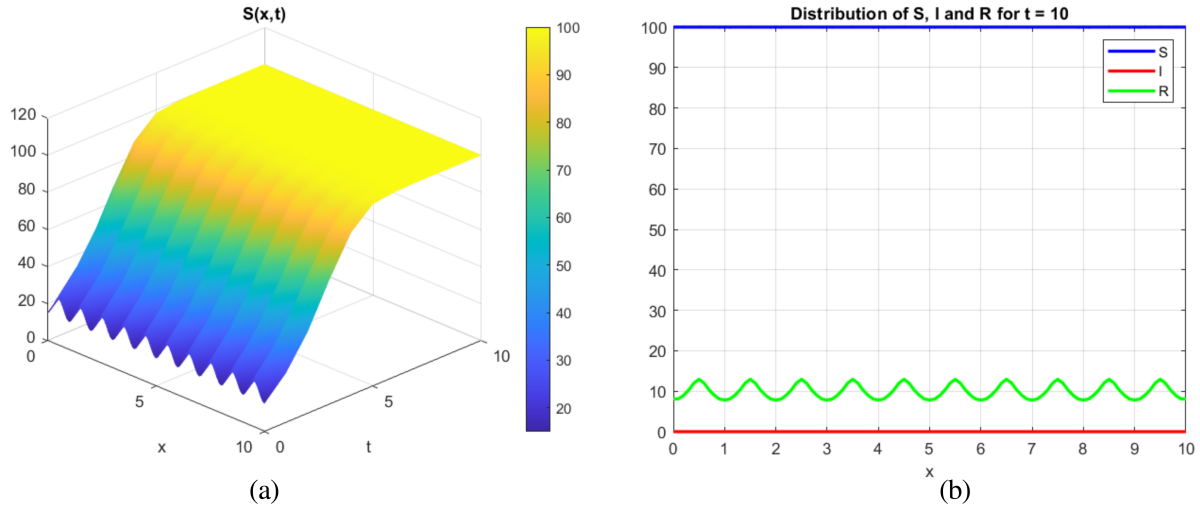

FIGURE 7 | Solution of system (1) with nonstandard Euler method (20), step-size function (27), and $\Delta t = 1$. (a) Time variation of the distribution of susceptible population, (b) Distribution of S, I and R for $t = 10$.

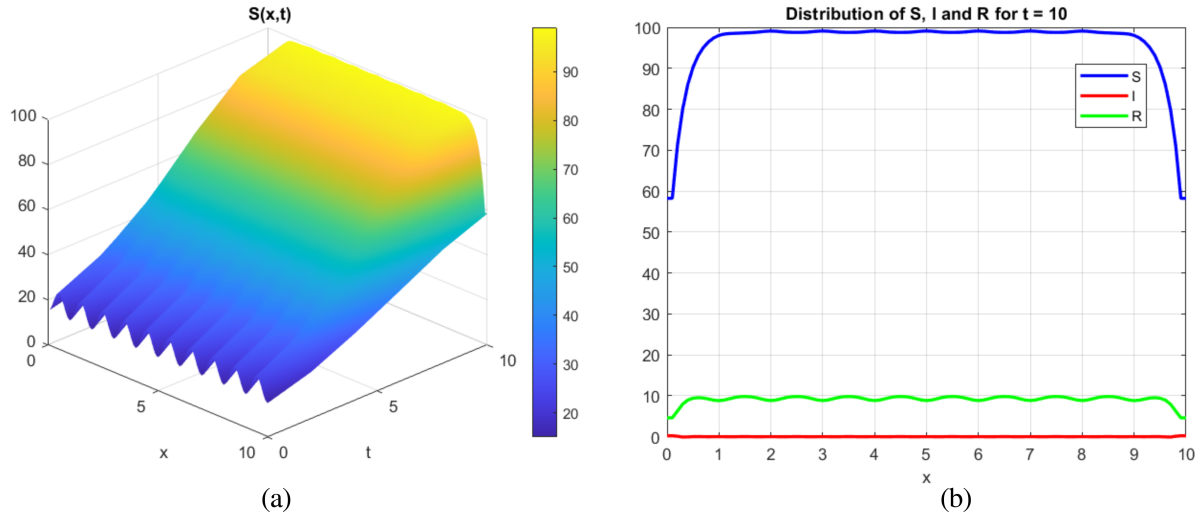

FIGURE 8 | Solution of system (1) with nonstandard semi-implicit Crank–Nicolson method (20), step-size function (27), and $\Delta t = 2$. (a) Time variation of the distribution of susceptible population, (b) distribution of S, I, and R for $t = 10$.

The same experiment is now performed using the Mickens' nonstandard semi-implicit Crank–Nicolson method with $\Delta t = 2$. As shown in Figure 8a,b, the solution remains positive. In this case, we have $H_2 = 1.99$ defined in equation (13), and $c = 1.05 \times 10^1$.

Remark 4.1. A comparison between the theoretical results in Theorem 1 and Lemma 1, as well as Figures 4 and 5, indicates that the Mickens-type nonstandard Euler method is more efficient than the exponential Euler method in preserving the positivity property for any time step size.

Remark 4.2. The Mickens-type nonstandard Forward Euler method with step-size functions (21) and (27) produces very similar results, as can be observed in Figures 5 and 7, although the corresponding the runtime differs. The same behavior is also observed for the semi-implicit Crank–Nicolson method. Tables 1 and 2 report the execution times obtained in each case, from which it is clear that the exponential step-size function consistently leads to faster computations.

Table 1 demonstrates that the step-size function (27) is computationally more efficient than the rational step-size function (21) when applied to the non-standard Forward Euler method. Since step-size function (27) incorporates an exponential term, it allows for more efficient computation and results in significantly shorter runtimes. As the time step Δt decreases,

10991476, 0, Downloaded from https://onlinelibrary.wiley.com/doi/10.1002/mma.70610 by Helmholtz Zentrum Muenchen Deutsches Forschungszentrum, Wiley Online Library on [21/04/2026]. See the Terms and Conditions (https://onlinelibrary.wiley.com/terms-and-conditions) on Wiley Online Library for rules of use; OA articles are governed by the applicable Creative Commons License

TABLE 1 | Runtime of the nonstandard forward Euler (NS FE) method with the step-size functions $\Phi_C(\Delta t) = \frac{\Delta t}{1 + C\Delta t}$ (see (21)) and $\Phi_C(\Delta t) = \frac{1 - e^{-C\Delta t}}{C}$ (see (27)) with different time steps.

Δt/step-size function	$\Phi_C(\Delta t) = \frac{\Delta t}{1 + C\Delta t}$	$\Phi_C(\Delta t) = \frac{1 - e^{-C\Delta t}}{C}$
$\Delta t = 2$	$6.68 \times 10^{-3} s$	$1.01 \times 10^{-3} s$
$\Delta t = 1$	$7.28 \times 10^{-3} s$	$1.09 \times 10^{-3} s$
$\Delta t = 0.1$	$1.00 \times 10^{-2} s$	$3.87 \times 10^{-3} s$
$\Delta t = 0.01$	$3.02 \times 10^{-2} s$	$2.09 \times 10^{-2} s$

TABLE 2 | Runtime of the nonstandard Crank–Nicolson (NS CN) method with the step-size functions (21)–(27) and different time steps.

Δt / Step-size function	$\Phi_C(\Delta t) = \frac{\Delta t}{1 + C\Delta t}$	$\Phi_C(\Delta t) = \frac{1 - e^{-C\Delta t}}{C}$
$\Delta t = 2$	$9.28 \times 10^{-3} s$	$2.40 \times 10^{-3} s$
$\Delta t = 1$	$9.45 \times 10^{-3} s$	$7.39 \times 10^{-3} s$
$\Delta t = 0.1$	$1.23 \times 10^{-2} s$	$1.19 \times 10^{-2} s$
$\Delta t = 0.01$	$2.04 \times 10^{-2} s$	$1.91 \times 10^{-2} s$

the runtime increases for both step-size functions, which is expected since smaller steps require more iterations to reach the final simulation time. Across all tested time steps, function (27) consistently yields shorter runtimes than function (21). The performance gap is particularly significant for larger time steps: at $\Delta t = 2$ and $\Delta t = 1$, function (27) is approximately 6.7 times faster. For smaller time steps, the runtime difference becomes less pronounced—function (27) is roughly 2.6 times faster at $\Delta t = 0.1$ and about 1.4 times faster at $\Delta t = 0.01$. These results indicate that the exponential-based step-size function (27) offers significantly better computational efficiency, especially for larger Δt. Although, its advantage decreases as the time step becomes smaller, it remains the more efficient option across all cases.

Table 2 demonstrates that the step-size function (27) is computationally more efficient than the rational step-size function (21) when applied to the non-standard Crank–Nicolson method. As the time step Δt decreases, the runtime increases for both step-size functions, which is expected since smaller steps require more iterations to reach the final simulation time. For all tested time steps, function (27) consistently produces shorter runtimes than function (21), though the performance gap is less pronounced compared to the Forward Euler method. At $\Delta t = 2$, function (27) is approximately 3.9 times faster than function (21), while at $\Delta t = 1$, it is about 1.3 times faster. At smaller time steps, the difference in runtime between the two functions becomes minimal. For instance, at $\Delta t = 0.1$, function (27) is only slightly faster, and at $\Delta t = 0.01$, both functions exhibit nearly the same performance. These results indicate that the exponential-based step-size function (27) improves computational efficiency for the Crank–Nicolson method, particularly for larger Δt. As the time step decreases, the efficiency gain becomes negligible, but function (27) still maintains a slight advantage.

Tables 1 and 2 compare the runtimes of the non-standard Forward Euler (NS FE) and Crank–Nicolson (NS CN) methods using step-size functions (21) and (27) across various time steps Δt. In both methods, runtime increases as Δt decreases due to the higher number of iterations required. The exponential step-size function (27) consistently yields shorter runtimes than the rational function (21). Overall, the NS FE method demonstrates higher computational efficiency than the NS CN method, as it requires fewer computational steps, especially at larger time steps and when using (27). For example, at $\Delta t = 2$, NS FE with (27) is about 2.4 times faster than NS CN, and at $\Delta t = 1$, it is nearly 6.8 times faster. With (21), the difference is smaller but NS FE remains faster. At smaller Δt, runtimes of both methods converge, with minimal differences between step-size functions. In these cases, NS CN with (27) can occasionally be marginally faster. In summary, the NS FE method combined with the exponential step-size function (27) demonstrates the highest overall computational efficiency, particularly for larger time steps. As Δt decreases, the performance differences among the methods and step-size functions become negligible. Given that both methods are first-order accurate, the NS FE method with the exponential step-size function (27) offers a more practical choice for long-term simulations of dynamical systems, as it can significantly reduce computation time.

10991476, 0, Downloaded from https://onlinelibrary.wiley.com/doi/10.1002/mma.70610 by Helmholtz Zentrum Muenchen Deutsches Forschungszentrum, Wiley Online Library on [21/04/2026]. See the Terms and Conditions (https://onlinelibrary.wiley.com/terms-and-conditions) on Wiley Online Library for rules of use; OA articles are governed by the applicable Creative Commons License

5 | Conclusion

In this work, we explored a diffusive SIR model governed by a system of semilinear PDEs. While the analytical properties such as well-posedness and positivity of the solutions were briefly addressed in the appendix, the core of the study focused on the numerical investigation of the model using various time integration methods. We implemented and compared the standard forward Euler, semi-implicit Crank–Nicolson methods with their Mickens-type nonstandard counterparts, as well as explicit exponential Runge-Kutta methods. Our analysis emphasizes the importance of positivity preservation, which is essential for ensuring biologically meaningful solutions. Numerical experiments demonstrate that, while the standard and exponential methods require time-step restrictions to preserve positivity, the Mickens-type nonstandard schemes retain this property unconditionally. These results demonstrate that the Mickens-type Nonstandard Finite Difference (NSFD) methods preserve positivity unconditionally, even for relatively large time step sizes Δt. This property is crucial for the reliable simulation of long-term dynamical systems, such as biological or epidemiological models, where negative populations or concentrations are not physically meaningful. Furthermore, our runtime comparisons between the two step-size functions, (21) and (27), show that while both satisfy the necessary theoretical conditions, the exponential-based function (27) consistently delivers superior computational efficiency. Specifically, it achieves faster runtimes across all tested scenarios without sacrificing accuracy or altering the qualitative behavior of the solutions. Notably, the Mickens-type nonstandard Forward Euler method combined with (27) demonstrates the best runtime performance—especially for larger time steps—outperforming both the rational step-size function and the Mickens-type nonstandard Crank–Nicolson method, even though all methods are first-order accurate. As Δt decreases, the runtime differences between methods and step-size functions become less significant, yet (27) remains the more efficient choice overall. Therefore, while both step-size functions yield equivalent numerical and analytical results, the exponential function (27) is preferable for simulations requiring long time horizons or large-scale computations, as its exact solution explicitly incorporates all time step sizes, providing a clear computational advantage. To conclude, the NS FE method paired with the exponential step-size function (27) achieves superior computational efficiency, especially when using larger time steps. As the time step size Δt becomes smaller, the efficiency differences between the various methods and step-size functions diminish. Since both approaches are first-order accurate, using the NS FE method with the exponential step-size function (27) proves to be a more efficient option for long-term dynamical system simulations, offering notable savings in computational time. This study represents a starting point for a broader research project. In future developments, we plan to extend this numerical approach to more complex and realistic models, such as those including additional compartments, time delays, or stochastic effects, which are often relevant in epidemiological contexts. We also plan to investigate the extension of the proposed framework to other contexts, like nonlocal models involving fractional operators, as well as quasilinear PDEs, for example p-Laplacian. A key objective will be to analyze and prove positivity preservation properties for these models, with particular attention to the design and validation of Mickens-type nonstandard finite difference methods that ensure the qualitative reliability of the numerical solutions.

Author Contributions

Rahele Mosleh: conceptualization; investigation; writing – original draft; methodology; validation; writing – review and editing; formal analysis; project administration; supervision; resources. **Claudia Panico:** conceptualization; investigation; writing – original draft; methodology; validation; visualization; writing – review and editing; software; project administration; resources. **Messoud Efendiyev:** conceptualization; investigation; methodology; validation; resources; supervision.

Acknowledgments

We express our sincere appreciation to Dr. Yiannis Hadjimichael for his valuable feedback and comments on this project. This work has no conflict of interest and there are no funders to disclose for this submission.

Data Availability Statement

The authors have nothing to report.

References

1. V. Capasso and G. Serio, "A Generalization of the Kermack-Mckendrick Deterministic Epidemic Model," *Mathematical Biosciences* 42, no. 1 (1978): 43–61.

2. J. Murray, *Mathematical Biology II: Spatial Models and Biomedical Applications*, 3rd ed. (Springer, 2003).

3. A. Okubo and S. A. Levin, *Diffusion and Ecological Problems: Modern Perspectives*, vol. 14 (Springer Science & Business Media, 2002).

10991476, 0, Downloaded from https://onlinelibrary.wiley.com/doi/10.1002/mma.70610 by Helmholtz Zentrum Muenchen Deutsches Forschungszentrum, Wiley Online Library on [21/04/2026]. See the Terms and Conditions (https://onlinelibrary.wiley.com/terms-and-conditions) on Wiley Online Library for rules of use; OA articles are governed by the applicable Creative Commons License

4. B. Takács and Y. Hadjimichael, "High Order Discretization Methods for Spatial-Dependent Epidemic Models," *Mathematics and Computers in Simulation* 198 (2022): 211–236.

5. L. J. S. Allen, *An Introduction to Stochastic Epidemic Models* (Springer Berlin Heidelberg, 2008), 81–130.

6. N. Wang, L. Zhang, and Z. Teng, "A Reaction-Diffusion Model for Nested Within-Host and Between-Host Dynamics in an Environmentally-Driven Infectious Disease," *Journal of Applied Analysis and Computation* 11, no. 4 (2021): 1898–1926.

7. W. Hundsdorfer and J. G. Verwer, *Numerical Solution of Time-Dependent Advection-Diffusion-Reaction Equations*, vol. 33 (Springer Science & Business Media, 2007).

8. K. W. Morton and D. F. Mayers, *Numerical Solution of Partial Differential Equations: An Introduction*, 2nd ed. (Cambridge University Press, 2005).

9. M. Berger and P. Colella, "Local Adaptive Mesh Refinement for Shock Hydrodynamics," *Journal of Computational Physics* 82, no. 1 (1989): 64–84.

10. D. Kuzmin, R. Löhner, and S. Turek, *Flux-Corrected Transport: Principles, Algorithms, and Applications* (Springer Science & Business Media, 2012).

11. K. Fellner and V. A. Kovtunenko, "A Singularly Perturbed Nonlinear Poisson-Boltzmann Equation: Uniform and Super-Asymptotic Expansions," *Mathematical Methods in the Applied Sciences* 38, no. 16 (2015): 3575–3586.

12. V. A. Kovtunenko and A. V. Zubkova, "On Generalized Poisson-Nernst-Planck Equations With Inhomogeneous Boundary Conditions: A-Priori Estimates and Stability," *Mathematical Methods in the Applied Sciences* 40, no. 6 (2017): 2284–2299.

13. U. M. Ascher, S. J. Ruuth, and R. J. Spiteri, "Implicit-Explicit Runge-Kutta Methods for Time-Dependent Partial Differential Equations," *Applied Numerical Mathematics* 25, no. 2 (1997): 151–167.

14. R. E. Mickens, *Nonstandard Finite Difference Models of Differential Equations* (World Scientific, 1993).

15. R. E. Mickens, "Nonstandard Finite Difference Schemes for Differential Equations," *Journal of Difference Equations and Applications* 8, no. 9 (2002): 823–847.

16. R. Anguelov, Y. Dumont, and J. Lubuma, "Mathematical Modeling of Sterile Insect Technology for Control of Anopheles Mosquito," *Computers & Mathematics With Applications* 64, no. 3 (2012): 374–389.

17. M. T. Hoang and M. Ehrhardt, "A Dynamically Consistent Nonstandard Finite Difference Scheme for a Generalized SEIR Epidemic Model," *Journal of Difference Equations and Applications* 30, no. 4 (2024): 409–434.

18. M. M. Khalsaraei, A. Shokri, S. Noeiaghdam, and M. Molayi, "Nonstandard Finite Difference Schemes for an Sir Epidemic Model," *Mathematics* 9, no. 23 (2021): 3082.

19. B. Buonomo, E. Messina, C. Panico, and A. Vecchio, "A Stable Numerical Method for Integral Epidemic Models With Behavioral Changes in Contact Patterns," *Electronic Transactions on Numerical Analysis* 61 (2024): 137–156.

20. B. Buonomo, E. Messina, C. Panico, and A. Vecchio, "An Integral Renewal Equation Approach to Behavioural Epidemic Models With Information Index," *Journal of Mathematical Biology* 90, no. 8 (2025): 1–26.

21. E. Messina, M. Pezzella, and A. Vecchio, "A Non-Standard Numerical Scheme for an Age-Of-Infection Epidemic Model," *Journal of Computational Dynamics* 9, no. 2 (2022): 239–252.

22. A. Duvnjak and H. J. Eberl, "Time-Discretization of a Degenerate Reaction-Diffusion Equation Arising in Biofilm Modeling," *ETNA. Electronic Transactions on Numerical Analysis* 23 (2006): 15–37.

23. H. J. Eberl and L. Demaret, "A Finite Difference Scheme for a Degenerated Diffusion Equation Arising in Microbial Ecology," *Electronic Journal of Differential Equations* 2007 (2007): 77–95.

24. E. Avila-Vales, G. E. Garcia-Almeida, and A. G. Perez, "Qualitative Analysis of a Diffusive SIR Epidemic Model With Saturated Incidence Rate in a Heterogeneous Environment," *Journal of Mathematical Analysis and Applications* 503, no. 1 (2021): 125295.

25. X. Tang and Y. Chen, "Analysis of the Diffusion SIR Epidemic Model With Networked Delay and Nonlinear Incidence Rate," *Journal of Mathematics* 2024, no. 1 (2024): 5739758.

26. R. E. Mickens, "Calculation of Denominator Functions for Nonstandard Finite Difference Schemes for Differential Equations Satisfying a Positivity Condition," *Numerical Methods for Partial Differential Equations* 23, no. 3 (2007): 672–691.

27. I. Faragó and R. Mosleh, "Some Qualitative Properties of the Discrete Models for Malaria Propagation," *Applied Mathematics and Computation* 439 (2023): 127628.

28. M. Efendiev, *Evolution Equations Arising in the Modelling of Life Sciences*, vol. 163 (Springer Science & Business Media, 2013).

29. M. Efendiev and V. Vougalter, *On the Necessary Conditions for Preserving the Nonnegative Cone: Mixed Diffusion* (Springer Singapore, 2021), 185–192.

30. M. Efendiev and V. Vougalter, *Verification of Biomedical Processes With Anomalous Diffusion, Trans-Port and Interaction of Species* (Springer Singapore, 2021), 65–74.

10991476, 0, Downloaded from https://onlinelibrary.wiley.com/doi/10.1002/mma.70610 by Helmholtz Zentrum Muenchen Deutsches Forschungszentrum, Wiley Online Library on [21/04/2026]. See the Terms and Conditions (https://onlinelibrary.wiley.com/terms-and-conditions) on Wiley Online Library for rules of use; OA articles are governed by the applicable Creative Commons License

Appendices

This section provides supplementary information that supports and expands upon the material presented in the main sections.

Appendix A

Analytical Analysis

In this section, we turn our attention to the analysis of the total population size of model (1), denoted by $N(t)$. Specifically, we consider the sum of all population compartments and examine its evolution over time by integrating the system over the spatial domain. We define

$$N(0) = \int_\Omega S(z,0) + I(z,0) + R(z,0)\, dz,$$

to be the total number of individuals in Ω at $t = 0$. Then, we have

$$N(t) = \int_\Omega S(z,t) + I(z,t) + R(z,t)\, dz \quad \text{for all } t \geq 0. \tag{A1}$$

Summing equations of system (1), we obtain

$$\frac{\partial S}{\partial t} + \frac{\partial I}{\partial t} + \frac{\partial R}{\partial t} = (d_S \Delta S + d_I \Delta I + d_R \Delta R) + rS\left(1 - \frac{S}{K}\right) - dI - \mu(S + I + R). \tag{A2}$$

From the second Green's Identity given by:

$$\int_\Omega u\Delta v\, dV = \int_\Omega \nabla u \cdot \nabla v\, dV - \int_{\partial\Omega} u\frac{\partial v}{\partial n}\, d\sigma,$$

we have

$$\int_\Omega (d_S \Delta S + d_I \Delta I + d_R \Delta R)\, dz = \int_{\partial\Omega} \left(d_S \frac{\partial S}{\partial n} + d_I \frac{\partial I}{\partial n} + d_R \frac{\partial R}{\partial n}\right) d\sigma = 0.$$

By integration from both sides of equation (A2) we have:

$$\frac{\partial}{\partial t}\int_\Omega (S(z,t) + I(z,t) + R(z,t))\, dz = \int_\Omega \left(rS\left(1 - \frac{S}{K}\right) - dI\right) dz - \mu \int_\Omega (S(z,t) + I(z,t) + R(z,t))\, dz.$$

Applying the definition of the total population size $N(t)$ as given in (A1), we obtain the following.

$$\frac{\partial N}{\partial t} + \mu N(t) = A,$$

where $A = \int_\Omega \left(rS\left(1 - \frac{S}{K}\right) - dI\right) dz$. Next, by easy calculation we attain

$$N(t) = \int_0^t \left(\int_\Omega \left(rS\left(1 - \frac{S}{K}\right) - dI\right) dz\right) e^{\mu(q-t)}\, dq + N(0)e^{-\mu t}.$$

Remark A.1. Note if $rS\left(1 - \frac{S}{K}\right) - dI = 0$ then $N(t)$ is a decreasing function that vanishes in the long run.

Appendix B

Analytically: Well-Posedness, Positivity-Preserving and Stability

In this section, we aim to analyze system (1) analytically, focusing on well-posedness and the positivity-preserving property of its solutions. The well-posedness of the model is established following the approach in [24]. As the classical maximum principle does not apply in this context, we adopt an alternative approach based on the technique detailed in [28].

Positivity of Solution With Neumann Boundary Condition

The aim of this section is to verify the *positivity* (i.e., non-negativity) of a class of equations involving diffusion, transport, and species interaction. By convention, we use the term *positivity* to refer to non-negativity. Although the term *non-negativity* might be more precise, we hope this convention will not cause confusion. Accordingly, we consider a system of reaction-diffusion-transport equations of

10991476, 0, Downloaded from https://onlinelibrary.wiley.com/doi/10.1002/mma.70610 by Helmholtz Zentrum Muenchen Deutsches Forschungszentrum, Wiley Online Library on [21/04/2026]. See the Terms and Conditions (https://onlinelibrary.wiley.com/terms-and-conditions) on Wiley Online Library for rules of use; OA articles are governed by the applicable Creative Commons License

parabolic type. For simplicity, we restrict the spatial domain to $\Omega = (0,1)$ and impose a single type of boundary condition—either Dirichlet or Neumann. Hence, we consider

$$\begin{cases} \frac{\partial u_1}{\partial t} = a_{11}\frac{\partial^2 u_1(t,x)}{\partial x^2} + a_{12}\frac{\partial^2 u_2(t,x)}{\partial x^2} + \gamma_{11}\frac{\partial u_1}{\partial x} + \gamma_{12}\frac{\partial u_2}{\partial x} + f_1(u_1,u_2) \\ \frac{\partial u_2}{\partial t} = a_{21}\frac{\partial^2 u_1(t,x)}{\partial x^2} + a_{22}\frac{\partial^2 u_2(t,x)}{\partial x^2} + \gamma_{21}\frac{\partial u_1}{\partial x} + \gamma_{22}\frac{\partial u_2}{\partial x} + f_2(u_1,u_2) \end{cases} \tag{B1}$$

$$u_1(0,x) = u_{10}(x), \quad u_2(0,x) = u_{20}(x), \quad x \in (0,1),$$

$$u_1'(t,0) = u_1'(t,1) = 0, \quad \text{and} \quad u_2'(t,0) = u_2'(t,1) = 0, \quad \forall t > 0.$$

To ensure parabolicity, we assume that $A + A^* > 0$, where A is the matrix and A^* is the conjugate

$$A := \begin{pmatrix} a_{11} & a_{12} \\ a_{21} & a_{22} \end{pmatrix}$$

It is worth noting that $a_{ij},\ i,j = 1,2$ are real numbers. Our goal is to present necessary and sufficient conditions for non-negativity of solutions of system (B1) if $u_{10}(x) \geq 0$ and $u_{20}(x) \geq 0$.

Theorem 4. *Let $(u_1(t,x), u_2(t,x))$ be a solution of (B1) and $u_1(0,x) \geq 0,\ u_2(0,x) \geq 0$. For $u_1(t,x) \geq 0$ and $u_2(t,x) \geq 0$ to be held, the necessary and sufficient conditions are the following.*

1. The matrix $A = (a_{ij})_{i,j=1}^2$ must be diagonal.
2. The matrix $\gamma = (\gamma_{ij})_{i,j=1}^2$ must be diagonal.
3. $f_1(0,u_2) \geq 0$ for all $u_2 \geq 0$ and $f_1(u_1,0) \geq 0$ for all $u_1 \geq 0$.

Remark 1. We are here not interested in the well-posedness of (B1). For this semilinear parabolic system there are a lot of results (see [24]) providing well-posedness. Therefore, in what follows, we assume that (B1) has a solution $(u_1(t,x), u_2(t,x))$ locally or globally for any $u_{10}(x), u_{20}(x) \geq 0$.

Remark 2. Theorem 4 holds, when domain Ω is a unbounded domain in $\mathbb{R}^n$.

Remark 3. Theorem 4 needs to be modified when instead of constant coefficients a_{ij} is considered density dependent coefficients $a_{ij}(u_1,u_2)$, $i,j = 1,2$.

Remark 4. The proof of Theorem 4 can be readily extended to cases involving the fractional Laplacian [29, 30] or the incorporation of a behavioral model [20]. Furthermore, Theorem 4 remains applicable to coupled PDE-ODE systems as well.

Remark 5. At present, there exists a sufficient condition under which the first assumption of Theorem 4 (as well as its quasilinear counterpart) holds, provided that

$$(u_{10}(x), u_{20}(x)) \geq 0 \text{ if } (u_1(t,x), u_2(t,x)) \geq 0.$$

Let $(u_{10}(x), u_{20}(x))$ be such initial data for which there exists $V(x) = (V_1(x), V_2(x))$ such that

$$\int_\Omega [u_{10}(x)V_1(x) + u_{20}(x)V_2(x)]\, dx = 0. \tag{B2}$$

Proof. Proof of Theorem 4 Since we assume that for any non-negative initial data, the solution $(u_1(t,x), u_2(t,x))$ remains non-negative, let us consider the specific initial conditions $(\tilde{u}(x), 0)$ and $V(x) = (0, \tilde{V}(x))$, where $\tilde{u}(x) \geq 0$ and $\tilde{V}(x) \geq 0$ are arbitrary real-valued functions. It is clear that the pairs $(\tilde{u}(x), 0)$ and $(0, \tilde{V}(x))$ satisfy equation (B2). Given our assumption that the solution remains non-negative for all non-negative initial data $(u_{10}(x), u_{20}(x)) \geq 0$, it follows that

$$\left(\frac{\partial u_2(t,x)}{\partial t}\Big|_{t=0}, \tilde{V}(x)\right)_{L^2(\Omega)} = \left(\lim_{t\to 0}\frac{u_2(t,x)}{t}, \tilde{V}(x)\right)_{L^2(\Omega)} \geq 0. \tag{B3}$$

On the other hand

$$\frac{\partial u_2(t,x)}{\partial t}\Big|_{t=0} = a_{21}\frac{\partial^2 \tilde{u}(x)}{\partial x^2} + \gamma_{21}\frac{\partial \tilde{u}(x)}{\partial x} + f_2(\tilde{u}(x), 0). \tag{B4}$$

Consequently, (B3) and (B4) leads to

$$\int_\Omega \left[a_{21}\frac{\partial^2 \tilde{u}(x)}{\partial x^2} + \gamma_{21}\frac{\partial \tilde{u}(x)}{\partial x} + f_2(\tilde{u}(x), 0)\right]\tilde{V}(x)\, dx \geq 0, \tag{B5}$$

10991476, 0, Downloaded from https://onlinelibrary.wiley.com/doi/10.1002/mma.70610 by Helmholtz Zentrum Muenchen Deutsches Forschungszentrum, Wiley Online Library on [21/04/2026]. See the Terms and Conditions (https://onlinelibrary.wiley.com/terms-and-conditions) on Wiley Online Library for rules of use; OA articles are governed by the applicable Creative Commons License

for all $\tilde{V}(x) \geq 0$, It is easy to see that, from (B5) it follows that, for any $\tilde{u}(x) \geq 0$ we have

$$a_{21}\frac{\partial^2 \tilde{u}(x)}{\partial x^2} + \gamma_{21}\frac{\partial \tilde{u}(x)}{\partial x} + f_2(\tilde{u}(x), 0) \geq 0 \quad \text{a.e. in } \Omega. \tag{B6}$$

□

Since equation (B6) holds for any $\tilde{u}(x) \geq 0$ almost everywhere in Ω, we may choose a specific form of $\tilde{u}(x)$ that attains its maximum at some point $x_0 \in (0, 1)$, and whose second derivative is arbitrarily negative. For instance, we consider the function

$$\tilde{u}(x) := e^{-\frac{1}{\varepsilon}(x-x_0)^2}.$$

It is easy to see that,

$$\frac{\partial \tilde{u}}{\partial x} = -\frac{2}{\varepsilon}(x - x_0)e^{-\frac{1}{\varepsilon}(x-x_0)^2}, \tag{B7}$$

$$\frac{\partial^2 \tilde{u}(x)}{\partial x^2} = -\frac{2}{\varepsilon}e^{-\frac{1}{\varepsilon}(x-x_0)^2} + \frac{4}{\varepsilon^2}(x - x_0)^2 e^{-\frac{1}{\varepsilon}(x-x_0)^2}.$$

Hence,

$$\left.\frac{\partial \tilde{u}}{\partial x}\right|_{x=x_0} = 0, \quad \left.\frac{\partial^2 \tilde{u}(x)}{\partial x^2}\right|_{x=x_0} = -\frac{2}{\varepsilon}.$$

Since $\varepsilon > 0$ can be chosen arbitrarily small, this leads to a contradiction of inequality (B6) at the point $x_0 \in \Omega$. Next, we consider the function

$$u_\star(x) := e^{-\frac{1}{\varepsilon}(x-x_0)}, \tag{B8}$$

which results in $\gamma_{21} = 0$. By repeating the same argument with the initial data $(\tilde{u}(x), 0)$ replaced by $(0, \tilde{u}(x))$, we similarly obtain $a_{12} = 0$ and $\gamma_{12} = 0$.

10991476, 0, Downloaded from https://onlinelibrary.wiley.com/doi/10.1002/mma.70610 by Helmholtz Zentrum Muenchen Deutsches Forschungszentrum, Wiley Online Library on [21/04/2026]. See the Terms and Conditions (https://onlinelibrary.wiley.com/terms-and-conditions) on Wiley Online Library for rules of use; OA articles are governed by the applicable Creative Commons License